International Journal of Heat and Mass Transfer 68 (2014) 29–34

Contents lists available at ScienceDirect

International Journal of Heat and Mass Transfer

journal homepage: www.elsevier.com/locate/ijhmt

Boiling heat transfer on a simulated nuclear fuel rod with annular fins

M.P. Porto [a,c], A.C.L. Costa [a,b], L. Machado [a], R.N.N. Koury [a], P.R. Cetlin [a], C.F.M. Coimbra [c,*]

[a] Programa de Pós Graduação em Engenharia Mecânica da Universidade Federal de Minas Gerais, Belo Horizonte, MG, Brazil
[b] Centro de Desenvolvimento da Tecnologia Nuclear CDTN/CNEN, Belo Horizonte, MG, Brazil
[c] Department of Mechanical and Aerospace Engineering, Jacobs School of Engineering, Center for Energy Research, University of California San Diego, La Jolla, CA 92093, USA

ARTICLE INFO

Article history:
Received 29 June 2013
Received in revised form 4 September 2013
Accepted 4 September 2013
Available online 2 October 2013

Keywords:
Nuclear rods
Confined boiling
Internal generation
Nucleate boiling

ABSTRACT

This work describes an improved design for a nuclear fuel rod, which was developed using an experimental circuit that simulates the nuclear rod environment in a pressurized water reactor (PWR). The heat exchanger circuit runs atmospheric to high-pressure boiling water through an annular finned tube (153 fins), which is used to enhance confined heat transfer rates and guide the nucleate boiling process. Volumetric electrical generation (Joule effect) is used to simulate nuclear heating. As much as 48 kW of electrical power is dissipated at different pressure levels up to 40 bar. Under these experimental conditions, heat transfer coefficients of the order of 73,000 W m^{-2} K^{-1} are achieved. Our experimental results show that critical safety levels can be easily reached using this design approach. Several nucleate boiling correlations were compared with the controlled experimental data sets, and a modified functional form for the boiling heat transfer coefficient is proposed.

1. Introduction

The nuclear fuel is the consumable part of the fuel rod, which is typically formed by a column of sintered uranium dioxide pellets encapsulated in zirconium alloy tubes. Fuel rods used in commercial power reactors are generally considered to be very robust when operating under critical temperature levels because only a very small number of failures (which may or not imply leakage of radioactive material into the cooling circuit) are expected. The high level of engineering reliability of such rods was obtained through extensive research carried on by universities, research centers and by industrial manufacturers. Recent works studied the physical behavior of real and simulated fuel rods under the severe operational conditions found in newly proposed designs for nuclear power reactors, e.g. [1–3]. The main operational goal is to ensure that there is no dispersion of radioactively contaminated water into the cooling circuit. Two critical conditions may determine operational failure: melting by over-heating and over-pressuring of the water line [3].

Fig. 1 is a schematic view of a nuclear fuel rod simulator, and Table 1 shows the main components of the power circuit. Understanding the heat transfer process in the region between the rod, pressurized water and the pressure vessel is critical to the overall operation of the system. This region involves phase-changing water (predominantly nucleate boiling), as can be seen in the Fig. 1.

Many reduced order models for the complex physics of nucleate boiling have been suggested. Mikic and Rohsenow [4] micro convective model, the microlayer model of Cooper and Lloyd [5] and the line contact model of Stephan and Hammer [6] and Mitrovic [7] are good examples of such models. Demiray and Kim [8] conclude that micro convection is the main heat transfer mechanism during nucleate boiling, highlighting that transient conduction during the re-wetting process is also a critical contributor to the overall heat transfer rates.

A quantitative analysis of the boiling phenomenon follows pool boiling and flow boiling experiments. Flow boiling phenomena plays an important role in conventional PWR nuclear rods, because of the presence of forced convection [9]. In this specific experiment, the guide discs affect the flow boiling, causing a confined pattern, and pool boiling can be used accurately for determining the HTC. Rops et al. [10] have discussed pool boiling in confined conditions in greater details, observing an enhancement effect due to confinement. Fig. 2 represents a typical pool boiling curve during water phase change considering the heat flux and temperature difference (ΔT, between wall and saturated fluid), and a confined correspondent curve (as shown by Rops et al. [10]). When ΔT is higher than 5 °C the process of nucleate boiling takes place. As the heat flux increases in the nucleate boiling range, the number of nucleate sites increase highly for a relatively low variation on temperature, generating a higher heat transfer coefficient. Rops et al. [10] indicate that inside a confined recipient, heat flux can be 10 times greater than in unconfined recipients considering the

* Corresponding author. Address: University of California San Diego, Department of Mechanical and Aerospace Engineering, 9500 Gilman Drive 0411, La Jolla, CA 92093-0411, USA. Tel.: +1 (858) 534 4285.
E-mail address: ccoimbra@ucsd.edu (C.F.M. Coimbra).

0017-9310/$ - see front matter © 2013 Elsevier Ltd. All rights reserved.
http://dx.doi.org/10.1016/j.ijheatmasstransfer.2013.09.008

Nomenclature

β	contact angle, rad
Bo	Bond number, $\frac{s}{\sqrt{\frac{\sigma}{g(\rho_l-\rho_v)}}}$
c	specific heat capacity, J kg^{-1} K^{-1}
C	constant
C_1	constant from modified-Rohsenow relation, −0.151
C_2	constant from modified-Rohsenow relation, 0.533
C_g	boiling number
C_{sf}	Rohsenow's C_{sf} constant, 0.0133
C^*_{sf}	Pioro's C^*_{sf} constant, 1.503
Δ	finite difference
D	diameter, m
ϕ	heat flux, W m^{-2}
Fr	Froude number, $\frac{\phi^3}{\rho_l^2 h_{lv}^3 \mu_l g}$
G	mass flux, kg m^{-2} s^{-1}
HTC	heat transfer coefficient
k	conductivity, W m^{-1} K^{-1}
L	thickness, m
m	Pioro's m constant, −1.1
μ	viscosity, Pa s
n	Rohsenow's n constant, 1
P	pressure, kPa
Pr	Prandtl number
q''	heat flux, W m^{-2}
R	thermal resistance, W^{-1} m^2 K
r	roughness, 1 μm
Re	Reynolds number
ρ	density, kg m^{-3}
s	space between discs, 6 mm
σ	surface tension, N m^{-1}
T	temperature, K
w	uncertainty
We	Weber number, $\frac{\phi\mu_l}{\rho_l h_{lv}\sigma}$

Subscripts

a	average
b	bubbles
ext	external
f	function
i	independent variables
int	internal
l	saturated liquid
p	constant pressure
pw	pressure vessel wall
red	reduced
sat	saturation
sim	simulator
v	saturated vapor

same temperature. As represented schematically in the Fig. 2, the unconfined curve tends to be convex and the confined one tends to be concave [10]. The theoretical physical explanation to this fact is the difficulty for re-wetting process by liquid flow due to the vertical bubble chaotic flow motion in unconfined recipients, generating a lower coefficient of heat transfer than in a confined one. For confined recipients, there is a tendency of circular cyclic flow, facilitating the re-wetting process because colder liquid is pumped towards the heated surface, which generates a higher heat flux. When ΔT approaches the critical value, the quantity of nucleate sites becomes so large that the pattern observed in the unconfined flow becomes very similar to the confined flow patterns. Using similar criteria, the angular discs between the rod and the pressure vessel tend to organize the bubble flow, thus enhancing the process of heat exchange.

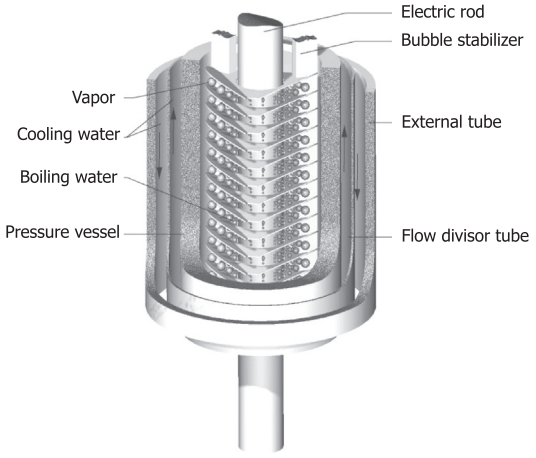

Fig. 1. Schematic view of a fuel rod, pressurized water, pressure vessel and cooling water circuit in the research simulator highlighting the flow divisor and the bubble stabilizer sections.

Table 1
Main components of the experimental loop.

System	Main function
Pressurized water	To enable heat transfer from the rod by nucleate boiling (Fig. 3)
Cooling water	To enable heat transfer from pressurized water by forced convection (Fig. 3)
Simulated fuel rod	To deliver Joule effect energy for simulating a nuclear fuel rod (Fig. 4)

On the one side, it is not expected a decreasing on the heat transfer coefficient (HTC, W m^{-2} K^{-1}) as consequence of the rod's vertical surface orientation [11]; on the other side, the vertical heated plate settles the flux upwards, parallel to the pressure vessel's wall surface, where it is located a great portion of the heat exchange surface area, and a lesser amount of heat (W) is transferred. On the other hand, the guiding fins emulate a confined environment; the annular discs force the flow in the direction of the pressure vessel wall, where bubbles condensate due to the lower temperature. Fig. 1 shows that the process of nucleate boiling in the present experiment occurs along the horizontal axis.

An experimental apparatus was built for studying the phenomena described above, with the goal of accomplishing the following objectives:

1. maintain the temperature of the pressure vessel for different ranges of pressurization (allowable temperature is 650 °C [12]);
2. determine the heat transfer coefficient for pressure levels of 1 bar, 5 bar, 10 bar and 40 bar;
3. compare different heat transfer coefficient relations with the data set, and suggest improvements in these correlations if necessary.

1.1. Experimental features

Fig. 3 presents the basic design of the experimental apparatus. Table 2 shows a list of experimental conditions for the fuel rod

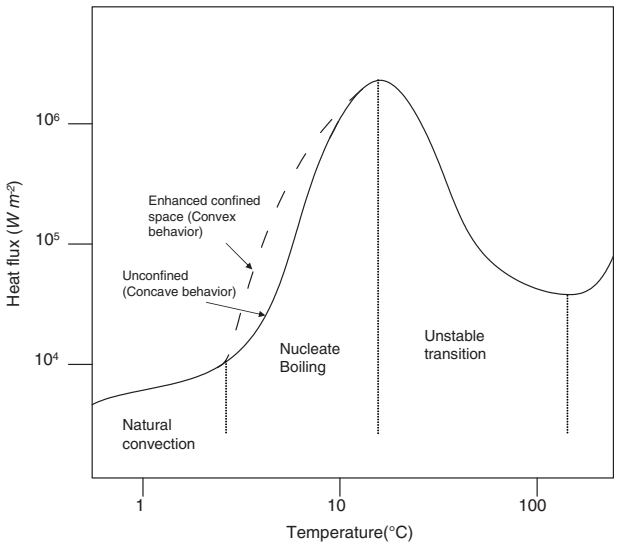

Fig. 2. Illustrative pool boiling curve highlighting differences between confined and unconfined spaces.

simulator and for the experimental device. The rod prototype is installed inside the first tube, and it is fitted with 153 annular flow guiding fins. This set is called the steam bubble stabilizer. The assembly was manufactured in stainless steel. The annular fins (guiding discs) must neither touch the external surface of the electric rod nor the internal surface of the pressure vessel. Heat is transferred from the rod by nucleate boiling process by advection. Condensation occurs when steam bubbles reach the pressure vessel inner surface. Outside there is a low pressure flow of water, which allows for convective cooling of the pressure vessel.

Between the external and the flow divisor pipes, water goes down through forced circulation imposed by the cooling water system. When the water reaches the bottom of the canal it turn direction and is pushed up along the external surface of the pressure vessel exchange heat with the experimental capsule at the pressure vessel.

The pressure vessel has its superior part, including flanges, manufactured in stainless steel AISI-304 and its inferior part manufactured in Al Mg[3] (aluminum alloy). The pressure vessel external diameter is 35.4 mm, its wall thickness is 4.2 mm and the total length is 1,092 mm. The pressure vessel is surrounded by the flow division tube and by an external tube, manufactured in stainless steel AISI-304.

The annular fin concept employed in this work has been used successfully by others [13,14]. Guide discs for directing the boiling process were first proposed by Neumann and collaborators at the Nuclear Research Centre, Julich, Germany, in 1968 [13].

Fig. 4 is a schematic depiction of the simulated fuel rod. The electrically heated rod is formed by a central core of ceramic material that includes a tubular resistive element, an electric insulation and a metallic wrapping tube. An Inconel-600 alloy was used for the resistive tubular element. The heated length of the rod is 600 mm and the maximum design power is 48 kW. The entire heated length was wrapped by the steam bubble stabilizer.

2. Experimental procedure

The following physical variables were measured: external temperatures of rod wrapping (4 thermocouples type-K); external temperatures of the pressure vessel (4 thermocouples type-K); input and output cooling water temperatures (2 thermocouples type-K); cooling water flow (Coriolis meter); pressurized water pressure (transmissor PT16); electric current and voltage at the rod simulator. The four thermocouples are distributed along the heated length and positioned at radial angles of 90°, disposed on the top region of the heating element, where the probability of critical heat flux is higher.

Each experimental run includes operation for 30 min at the pressure of 1 bar, to remove air from the experimental capsule.

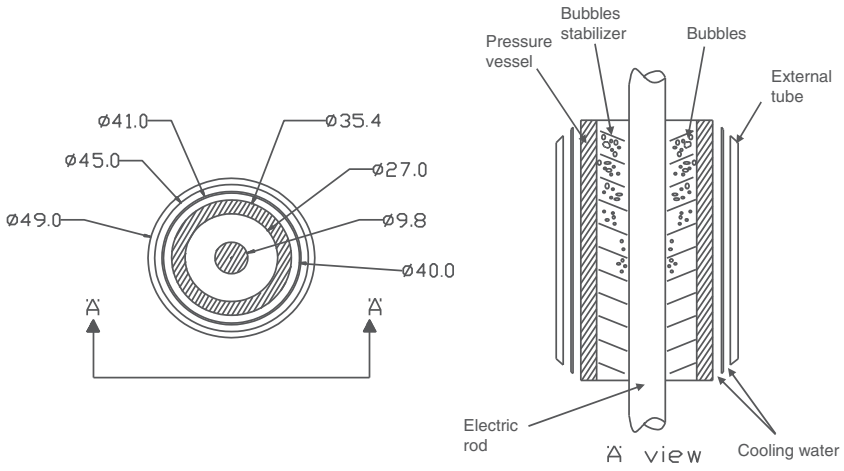

Fig. 3. Basic design of the experimental apparatus.

Table 2
Materials and dimensions used in the experimental setup.

Component	Material	Ext./Internal diameters (mm)/(mm)	Design temp. (°C)	Design pressure (bar)
Rod wrapping	Stainless steel	9.8/8	500	133
Pressure vessel	Stainless steel-Al alloy	35.4/ 27	122	133
Flow division tube	Stainless Steel	41/ 40	122	10
External tube	Stainless Steel	49/ 45	50	10
Guide disc	Stainless Steel	26/ 11	122	133

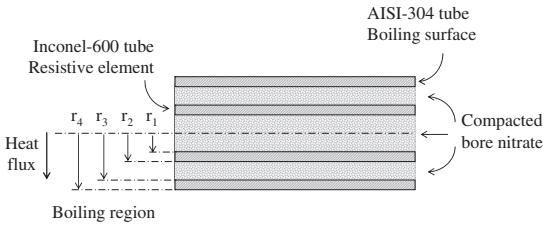

Fig. 4. Separate parts of the electric rod; $r_1 = 2$ mm, $r_2 = 2.6$ mm, $r_3 = 4$ mm, $r_4 = 4.9$ mm, Rod length = 600 mm.

Next, the experiments initiate according to the following procedure: (1) adjust the cooling water flow at 0.39 kg/s and the temperature of the cooling water at 30 °C; (2) adjust the water pressure to 1 bar, 5 bar, 10 bar or 40 bar (specific to each experiment); (3) adjust the electric current rectifier (thermal power) until reaching the value of thermal power, that is 20% smaller than the value of critical heat flow (determined by classical correlations); (4) record data for a period of 2 min.

The heat flux of typical nuclear fuel rods is well characterized by a chopped cosine distribution along the axial length [15]. This work considers uniform heat flow, which is a conservative assumption because all measurements were executed near the critical heat flow regime.

All instruments were calibrated with secondary standards. The overall uncertainty of each measurement results from a combination of the instrument uncertainty and the uncertainty of the adjusted calibration curve, and by the statistic uncertainty associated with the 2-min average of the measurements carried out by the data acquisition system. The calibration curves for all meters were determined by the least squares method for all experimental points. Uncertainties of the primary physical variables measured, such as temperature and pressure, and the water properties were obtained from [16]; the compound uncertainties for the thermal power and heat transfer coefficients were calculated using the compound chain rule of Eq. 1 below [17].

$$w_f = \sqrt{\left(\frac{\delta f}{\delta x_i} w_i\right)^2}, \tag{1}$$

where f is a function of i independent variables, w_f is the absolute uncertainty associated to the function f determined by the partial derivative of f and the uncertainties w_i associated to the independent variables. The expanded experimental heat transfer coefficient uncertainty can be found in Table 3.

3. Pool boiling and flow boiling relations

Several working correlations for pool boiling heat transfer coefficients have been proposed in the past few decades [4,18–28].

Rohsenow [21,22,24,25] and others have proposed a number of correlations that successfully capture the main physical processes of boiling. Pioro et al. [25] compared various correlations and concluded that the best results for water are obtained using Pioro [23] and Rohsenow [21,22]. Both of these correlations are used for comparison in this work, along with the correlation by Cooper [19], which is widely used in industry. The correlation developed recently by Souza [18] for confined flows at low pressures is also considered here. Table 4 shows the different relations as they were applied in this work.

Table 3
Results obtained for different conditions (1, 5, 10 and 40 bar).

P_{sat} (bar)	q'' (kW m^{-2})	T_{vessel} (°C)	T_{sim} (°C)	h (kW m^{-2} K)	w_f (%)
1	527	53.6	123	18.1	29
5	872	67.3	178	34.8	16
10	1075	74.2	202	48	10
40	1325	87.4	266	73	7.5

4. Results and discussion

Table 3 shows values of heat flux, maximum vessel temperature, maximum rod temperature, average heat transfer coefficient and uncertainty for 4 different pressures. The vessel internal temperature is higher than the external temperature, and because of this fact only the first one is presented. The internal temperature and heat transfer coefficient were calculated using Eqs. (2) and (3) respectively:

$$T_{int} = T_{ext} + q'' R_{pw}, \tag{2}$$

$$h = \frac{q''}{\Delta T_{sat}}, \tag{3}$$

where R_{pw} is the pressure vessel wall thermal resistance (L_{pw}/k_{pw}, with units of $K\ m^2 W^{-1}$) and ΔT_{sat} is the difference between the rod surface and the saturated fluid temperature (°C).

The highest vessel temperature occurs for the pressure of 40 bar, and it is approximately 87.4 °C. This value is substantially lower than the maximum allowable for the stainless steel pressure vessels (650 °C). The maximum experimental value obtained for the heat transfer coefficient in this configuration is 73 kW m^{-2} K^{-1}.

Fig. 5 is a scatter plot for all the relations defined in Table 4. The correlations by Cooper [19], Ribatski–Jabardo [20], Rohsenow [21,22] and Pioro [23] overestimate the values of temperature difference, which means that these correlations overestimate the heat transfer coefficient (HTC). The Jens–Lottes' relation [29] has the right trend but with larger spread but underestimates the HTC, especially at higher pressure. Similarly, the recently proposed correlation of Souza [18] captures the right HTC for low values of pressure, but overestimates the HTC for high pressure, which seems to indicate that this correlation overestimates the enhancement effect of confinement at higher pressures. Rohsenow's correlation is the most precise (albeit less accurate), and because of this higher precision, it was chosen as the basic functional form for a modified correlation that is valid for all range of parameters in this study, and that also takes into account the effect of the annular fins.

4.1. Modified-Rohsenow relation

Rohsenow's relation [21] assumes that the majority of the heat transferred during nucleate boiling comes from the heated surface to the saturated liquid, which allows us to parametrize the boiling Nusselt number as:

$$Nu_b = f(Re_b, Pr_l), \tag{4}$$

Table 4
Boiling heat transfer coefficient relations used in this work.

Author	Correlation
Souza [18]	$\Delta T = \frac{\phi S}{k_l(1.8510^{-9} FrWe^{-2.76} Bo^{-0.03})}$
Jens-Lottes [29]	$\Delta T = \frac{25^4 \phi}{e^{4P_{sat}/6.2}}^{1/4}$
Cooper [19]	$\Delta T = \frac{\phi}{55P_{red}^{0.12-0.2\log_{10}r_a}(-\log_{10}P_{red})^{-0.55}M^{-0.5}(\phi)^{0.67}}$
Ribatski-Jabardo [20]	$\Delta T = \frac{\phi}{f_w P_{red}^{0.45}(-\log_{10}P_{red})^{-0.8} r_a^{0.2} M^{-0.5}(\phi)^{0.9-0.3P_r^{0.2}}}$
Rohsenow [21,22]	$\Delta T = \frac{h_{lv}C_{sf}}{c_{p,l}}\left[\frac{\phi}{\mu_l h_{lv}}\sqrt{\frac{\sigma}{g(\rho_l-\rho_v)}}\right]^{0.33}\left(\frac{c_{p,l}\mu_l}{k_l}\right)^n$
Pioro [23]	$\Delta T = \frac{\phi}{\frac{k_l C_{sf*}}{l^*}\left[\frac{\phi}{h_{lv}\rho_v^{0.5}\sigma g(\rho_l-\rho_v)^{0.25}}\right]^{2/3}} Pr^m$

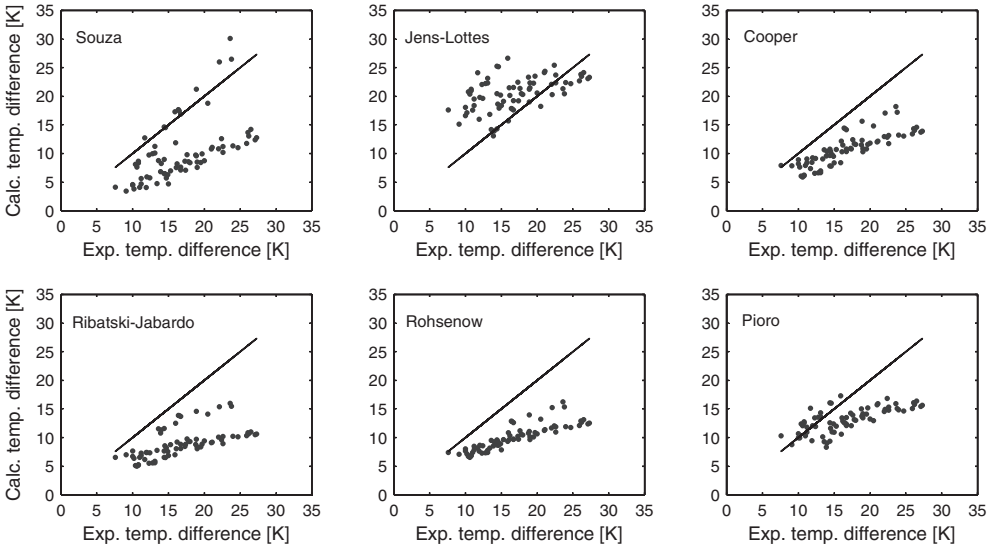

Fig. 5. Calculated and measured difference of temperature between the external rod surface and the boiling water flow for all pressure levels; Correlations by Souza [18], Jens–Lottes [29], Cooper [19], Ribatski–Jabardo [20], Rohsenow [21,22] and Pioro [23] are used to generate ΔT values for comparison with experimental values.

where Re_b is the bubble Reynolds number, and Pr_l is the Prandtl number for the saturated liquid. The bubble Reynolds number is:

$$Re_b = \frac{G_b D_b}{\mu_l}, \tag{5}$$

where G_b and D_b are the bubble mass flux and the bubble diameter, respectively. Rohsenow uses Fritz's [30] relation for determining the bubble diameter, as presented in Eq. 6, and calculates the mass flux by using the Eq. 7:

$$D_b = C_d \beta \sqrt{\frac{2\sigma}{g(\rho_l - \rho_v)}}, \tag{6}$$

$$G_b = \frac{\phi}{h_{lv} C_g}, \tag{7}$$

where C_g is the boiling number.

Substituting Eqs. 6 and 7 into Eq. 5, the bubble Reynolds number is obtained:

$$Re_b = \frac{\left(C_d \beta \sqrt{\frac{2\sigma}{g(\rho_l-\rho_v)}}\right)\left(\frac{\phi}{h_{lv} C_g}\right)}{\mu_l} = \frac{C_{sf}\beta\phi\sqrt{\frac{\sigma}{g(\rho_l-\rho_v)}}}{h_{lv}\mu_l}, \tag{8}$$

where $C_{sf} = \sqrt{2} C_d / C_g$, and β is a proportionality coefficient that was assumed to be unity in the original Rohsenow's relation.

More recently, Weckesser [31] and Luke [32] have presented new relations for the bubble diameter considering the same functional form as Fritz [30], but including the reduced pressure in the relation. Reduced pressure was also used by Schomann [33] in his bubble diameter relation. The reduced pressure concept is also used in our modified-Rohsenow relation for determining the bubble diameter:

$$D_b = P_{red}^{C_1} C_d \beta \sqrt{\frac{2\sigma}{g(\rho_l - \rho_v)}}. \tag{9}$$

The effect of the annular fins is captured by modification of the bubble Reynolds number exponent presented by Rohsenow (originally equal to 0.33 but now left as a parameter to be optimized, C_2).

The complete modified relation is thus

$$\Delta T = \frac{h_{lv} C_{sf}}{c_{p,l}} \left(\frac{\phi}{\mu_l h_{lv}} P_{red}^{C_1} \sqrt{\frac{\sigma}{g(\rho_l - \rho_v)}}\right)^{C_2} \frac{c_{p,l}\mu_l}{k_l}. \tag{10}$$

A genetic algorithm method is used to optimize the values of the two constants C_1 and C_2; the optimal values were found to be $C_1 = -0.151$, and $C_2 = 0.533$.

Fig. 6 presents a scatter plot comparing this modified relation with the experimental results. It is observed a good correlation mainly for smaller values of temperature difference, that corresponds to higher values of pressure, where the data is more accurate (see Table 3).

A comparison between theoretical and experimental errors is presented in Table 5, indicating that the modified relation proposed here is consistently more accurate and robust when com-

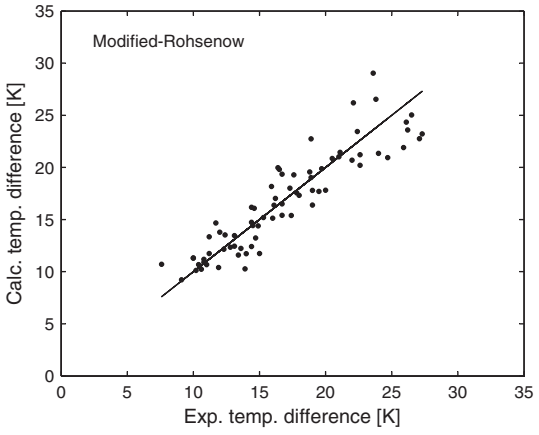

Fig. 6. Scatter plot for the proposed modified Rohsenow relation.

Table 5
Error metrics comparison between the methodologies employed for the data set.

Correlation	MAE (%)	RMSE (%)
Souza [18]	42.1	46.1
Jens-Lottes [29]	34.0	46.8
Cooper [19]	24.6	28.0
Ribatski-Jabardo [20]	38.6	41.5
Rohsenow [21,22]	38.4	41.5
Pioro [23]	23.2	26.1
Modified-Rohsenow	9.5	12.7

pared to the other relations for nucleate boiling at all pressure levels.

5. Conclusions

The geometry of fuel rods and pressure vessels play an important role in nuclear reactor safety. A common cause of failure is excessive heating due to inadequate levels of heat removal. A different geometric configuration consisting of a confined pressure vessel that is fitted with annular fins around the fuel rod is proposed here. The rod is heated through an electrical resistance array that dissipates up to 48 kW (simulating a PWR nuclear fuel rod). The annular fins guide the bubbles generated at the rod interface away from the rod in the axial direction to the cooling jacket, thus enhancing the heat flow even thought the fuel rod is oriented vertically.

The maximum temperature at the wall of the pressure vessel for this configuration and heat transfer rates was 87.4 °C, which is well below the maximum allowable of 650 °C. Heat transfer coefficients as high as 73 kW m^{-2} K^{-1} were observed during our experiments.

Several correlations for boiling heat transfer coefficients were compared to the experimental data sets corresponding to different pressures (1, 5, 10 and 40 bar). Most correlations (4 out of the 6 tested) underestimate the values of temperature difference, which means that the calculated heat transfer coefficients are higher than the actual value. A modification to the classic boiling heat transfer correlation suggested by Rohsenow to account for the effect of wall confinement, the annular fins (which guide the boiling flow away from the rod), and the high pressure levels of our experiments is proposed. The modified Rohsenow correlation proposed in this work achieves substantially better results in terms of both accuracy and precision for all pressure levels.

References

[1] Y. Jiang, Y. Cui, Y. Huo, S. Ding, Three-dimensional FEM analysis of the thermo-mechanical behaviors in the nuclear fuel rods, Ann. Nucl. Energy 38 (2011) 2581–2593.

[2] C.C. Liu, Y.M. Ferng, C.K. Shih, CFD evaluation of turbulence models for flow simulation of the fuel rod bundle with a spacer assembly, Appl. Therm. Eng. 40 (2012) 389–396.

[3] A.C.L. Costa, Desenvolvimento de um dispositivo experimental e determinação dos parâmetros de refrigeração por ebulição nucleada confinada para um circuito de irradiação a água fervente com a vareta combustível nuclear substituída por um simulador elétrico, Ph.D. thesis, Universidade Federal de Minas Gerais, Belo Horizonte, Brazil, 2003.

[4] B.B. Mikic, W.M. Rohsenow, A new correlation of pool-boiling data including the effect of heating surface characteristics, J. Heat Transfer 91 (1969) 245–250.

[5] M.G. Cooper, A.J.P. Lloyd, The microlayer in nucleate boiling, Int. J. Heat Mass Transfer 12 (1969) 895–913.

[6] P. Stephan, J. Hammer, A new model for nucleate boiling heat transfer, Wärme- und Stoffübertragung 30 (1994) 119–125.

[7] J. Mitrovic, Flow and heat transfer in the wedge-shaped liquid film formed during the growth of a vapour bubble, Int. J. Heat Mass Transfer 41 (1998) 1771–1785.

[8] F. Demiray, J. Kim, Microscale heat transfer measurements during pool boiling of FC-72: effect of subcooling, Int. J. Heat Fluid Flow 47 (2004) 3257–3268.

[9] L. Zou, Experimental study on subcooled flow boiling on heating surfaces with different thermal conductivities, Ph.D. thesis, University of Illinois at Urbana – Champaign, Urbana, Illinois, 2010.

[10] C.M. Rops, R. Lindken, J.F.M. Velthuis, J. Westerweel, Enhanced heat transfer in confined pool boiling, Int. J. Heat Fluid Flow 30 (4) (2009) 751–760.

[11] K. Nishikawa, Y. Fujita, Nucleate boiling heat transfer and its augmentation, Adv. Heat Transfer 27 (1984) 1559–1571.

[12] G. Towler, R. Sinnott, Chemical Engineering Design, 2nd ed., Butterworth-Heinemann, Boston, 2013.

[13] K. Reichardt, M. Newmann, Irradiation of water-cooled fuel rods in boiling water loops, Kerntechnik: J. Nucl. Eng. Sci. 6 (1968) 331–337.

[14] J.C. Whitehouse, Enhancement of pool boiling from a vertical rod using guide disks, in: Proceedings of the Fifth International Meeting on Reactor Thermal Hydraulics, 1992, pp. 981–989.

[15] F.J. Erbacher, H.J. Neitzel, K. Wiehr, Cladding deformation and emergency core cooling of a pressurized water reactor in a LOCA: summary description of the REBEKA program, KfK 4781, Kernforschungszentrum Karlsruhe, Karlsruhe, 1990.

[16] W. Wagner, A. Kruse, A. Properties of water and steam – the industrial standard IAPWS-IF97 for the thermodynamics properties, Springer, Berlin, 1998.

[17] S.J. Kline, F.A. McClintock, Describing uncertainties in single-sample experiments, Mech. Eng. (1953) 3–8.

[18] R. Souza, Estudo da ebulição confinada subresfriada em experimento para testes em microgravidade, Ph.D. thesis, Universidade Federal de Santa Catarina, Florianópolis, Brazil, 2010.

[19] M.G. Cooper, Heat flow rates in saturated nucleate pool boiling – a wide ranging examination using reduced properties, Adv. Heat Transfer 16 (1984) 157–238.

[20] G. Ribatski, J.M.S. Jabardo, Experimental study of nucleate boiling of halocarbon refrigerants on cylindrical surfaces, Int. J. Heat Mass Transfer 46 (2003) 4439–4451.

[21] W.M. Rohsenow, A method of correlating heat transfer data for surface boiling of liquids, Technical report no 5, M.I.T. Division of Industrial Cooperation, Cambridge, 1951.

[22] W.M. Rohsenow, J.P. Hartnett, Y.I. Cho, Handbook of Heat Transfer, third ed., McGraw-Hill, New York, 1998.

[23] I.L. Pioro, Boiling heat transfer characteristics of thin liquid, in: Preprints of the 10th International Heat Pipe Conference, Stuttgart, Germany, 1997, pp. 1–10.

[24] I.L. Pioro, W.M. Rohsenow, S.S. Doerffer, Nucleate pool-boiling heat transfer. I: Review of parametric effects of boiling surface, Int. J. Heat Mass Transfer 47 (2004) 5033–5044.

[25] I.L. Pioro, W.M. Rohsenow, S.S. Doerffer, Nucleate pool-boiling heat transfer. II: Assessment of prediction methods, Int. J. Heat Mass Transfer 47 (2004) 5045–5057.

[26] S.S. Kutateladze, V.M. Borishanskii, Concise Encyclopedia of Heat Transfer, Pergamon Press, Oxford, 1966.

[27] S.S. Kutateladze, Heat Transfer and Hydrodynamic Resistance: Handbook, Energoatomizdat Publishing House, Moscow, 1990.

[28] H.K. Forster, N. Zuber, Dynamics of vapor bubbles and boiling heat transfer, AIChE J. 1 (1955) 531–535.

[29] W.H. Jens, P.A. Lottes, An analysis of heat transfer, burnout, pressure drop and density data for high pressure water, ANL-4627, Argonne National Lab. Report, Chicago, 1951.

[30] W. Fritz, Berechnung des maximal volume von dampfblasen, Phys. Zeitschrift 36 (1935) 379–388.

[31] M. Weckesser, Untersuchungen zur blasenbildung beim Sieden in freier konvektion, Ph.D. thesis, Universität Karlsruhe, Karlsruhe, Germany, 2010.

[32] A. Luke, Interactions between bubble formation and heating surface in nucleate boiling, Exp. Therm. Fluid Sci. 35 (2011) 753–761.

[33] H. Schomann, Beitrag zum Einfluβ der Heizflächenrauhigkeit auf den Wärmeübergang beim Blasensieden, Ph.D. thesis, Universität Paderborn, Paderborn, Germany, 1994.